FLORE
Repository istituzionale dell'Università degli Studi di Firenze

Isotopic disequilibrium during anatexis: a case study of contact melting, Sierra Nevada, California

Questa è la Versione finale referata (Post print/Accepted manuscript) della seguente pubblicazione:

Original Citation:

Isotopic disequilibrium during anatexis: a case study of contact melting, Sierra Nevada, California / S. TOMMASINI; G.R. DAVIES. - In: EARTH AND PLANETARY SCIENCE LETTERS. - ISSN 0012-821X. - STAMPA. - 148:(1997), pp. 273-285. [10.1016/S0012-821X(97)00031-9]

Availability:

This version is available at: 2158/224187 since:

Published version:

DOI: 10.1016/S0012-821X(97)00031-9

Terms of use:

Open Access

La pubblicazione è resa disponibile sotto le norme e i termini della licenza di deposito, secondo quanto stabilito dalla Policy per l'accesso aperto dell'Università degli Studi di Firenze (https://www.sba.unifi.it/upload/policy-oa-2016-1.pdf)

Publisher copyright claim:

(Article begins on next page)

26 April 2024

ELSEVIER

Earth and Planetary Science Letters 148 (1997) 273–285

EPSL

Isotope disequilibrium during anatexis: a case study of contact melting, Sierra Nevada, California

Simone Tommasini *, Gareth R. Davies

Faculteit der Aardwetenschappen, Vrije Universiteit, De Boelelaan 1085, 1081 HV Amsterdam, The Netherlands

Received 22 October 1996; revised 11 February 1997; accepted 12 February 1997

Abstract

The geochemical consequences of contact melting were investigated in the Sierra Nevada Batholith, where trachyandesite magmas have intruded and melted the host granitic rocks. Partial melting of the granite varies from 10–20% at contact regions, to 50–70% in a granite block within the trachyandesite. Thermal modelling suggests that the temperature of the granite block exceeded its solidus within 3 months of trachyandesite intrusion, reached a maximum of ~ 1000°C after ca. 1.5 yr, and remained above 500°C for ca. 40 yr.

Sr, Nd and Pb isotope data of granitic melts record marked Sr isotope, and to a lesser extent Pb isotope, disequilibrium both within different glass fractions and between glasses and their source. Rb/Sr isochron calculations on residual mineral–glass pairs fail to yield the age of melting obtained by ^{40}Ar–^{39}Ar dating (11.9 Ma). Sr and Pb isotope data of glasses establish that major rock-forming minerals of the granite had not attained isotope equilibrium *before* the onset of melting. Consequently, the isotopic composition of the successive liquid fractions originating from granite melting depended on the relative contribution of each mineral to the elemental budget of the melts.

The extrapolation of these results to the petrogenesis of crustal melts and more generally to studies of crustal evolution, suggests that isotope disequilibrium during anatexis and high-grade metamorphism may be a common characteristic of many geologic settings. If future studies substantiate these results, some geochemical models of crustal melting and assimilation may need revision. In addition, marked Sr isotope disequilibrium in the residual mineral phases within the partially melted granite raises concerns about the reliability of radiometric dating in metamorphic terranes.

Keywords: radioactive isotopes; equilibrium; diffusion; anatexis; absolute age

1. Introduction

In the last decade a number of experiments have determined diffusion coefficients of key elements in major rock-forming minerals (see compilation in [1]). In particular, Sr diffusion coefficients in feldspar are low ($< 10^{-16}$ cm^2 s^{-1}) even at crustal anatectic temperatures (~ 750°C) [2–6]. This property has enabled the use of Sr isotopes both to date the timing and rate of mineral growth in a high-silica magma [7] and to constrain the nature of magma mixing in a rhyolitic magma [8]. Recent studies have demonstrated marked isotope disequilibrium during granite melting in the laboratory [9,10] and in the field [11]. Empirical studies have also established that the slow diffusion of Nd and Pb in garnet can be used to

* Corresponding author's present address: Dipartimento di Scienza del Suolo e Nutrizione della, Pianta, Piazzale delle Cascine 16. 50144 Firenze, Italy.

0012-821X/97/$17.00 Copyright © 1997 Elsevier Science B.V. All rights reserved.
PII S0012-821X(97)00031-9

determine prograde metamorphic ages, despite subsequent heating and long-lived cooling histories [12–17]. Overall, these studies demonstrate that garnet and feldspar remain isotopically closed systems with respect to their host at high temperatures (> 600°C). Isotope disequilibrium is commonly used in Pb isotope systematics to date inherited zircon cores (and other accessory minerals) in high-grade metamorphic rocks and crustal melts (e.g., [18–20]). Despite these observations, a full assessment has not been made of the consequences of minerals not attaining isotope equilibrium during metamorphism and anatexis.

Here we present a study of contact melting caused by the intrusion of a trachyandesite magma in a Cretaceous granite, northwest of Mono Lake, California. The melt–source relationship is clear and can be unequivocally identified in the field, since melts remained essentially in situ (i.e., within the volume of the outcrop). This fact provides us with an excellent natural laboratory to assess the extent of isotope (dis)equilibrium during anatexis, given that most exposed granitoids cannot be compared with their sources since they originated deep in the crust.

2. Geological background

The Rattlesnake Gulch granite is part of the Cretaceous Sierra Nevada Batholith and has a biotite K–Ar age of 92.9 ± 3.1 Ma [21]. It is directly overlain by the Late Miocene Rancheria Tuff Breccia, indicating it was already exposed on the surface prior to the onset of the Cenozoic basaltic magmatism (see Chesterman [21] for details). Two trachyandesite magmas have intruded and melted the granite [22]. They represent remnants of near-surface conduits through which magma flowed, and are part of the Rancheria Tuff Breccia [21]. Textural and geochemical relationships between granite melts and residual mineral phases have been discussed elsewhere [22,23] and only a brief review of field and petrographic characteristics is given here.

This study is focused on the western trachyandesite plug (see [21,23] for details on the location). The plug has an approximately circular shape, is roughly 50 m in diameter, and outcrops along the edge of a small valley surrounded by exposures of unmelted granite. The emplacement of the plug is probably related to a single magmatic event since there is no evidence of multiple injections. Field observations establish that granite melting along the contact was of relatively low degrees (10–20%) and limited to a narrow zone 2–3 m wide. A large block of granite, ~ 4 × 4 m in size, occurs within the plug and has experienced high degrees of melting (50–70%). The contacts between the block of partially melted granite and the trachyandesite are sharp, suggesting negligible interaction.

2.1. Petrography

The unmelted granite has a hypidiomorphic medium to coarse grained texture. It consists of quartz, andesine/oligoclase (core An_{40}, rim An_{15}), microperthitic orthoclase/microcline (Or_{90}) and biotite [mol Mg/(Mg + Fe) = 0.4], with accessory apatite, zircon, oxides and allanite. The partially melted granite has a hypocrystalline groundmass enclosing residual plagioclase, sanidine/anorthoclase, quartz and a fine-grained intergrowth of rutile, oxides and orthopyroxene from biotite breakdown, along with accessory zircon and apatite.

The onset of melting within the granite is very clear in the contact zone and is defined by the first appearance of glass at the boundaries between quartz and feldspar grains. The glass forms veins and pools that pervade feldspar and quartz grains and give the rims of feldspars a characteristic spongy texture (e.g., see SEM photographs in [22]). Biotite also reacts, breaking down to a very fine-grained intergrowth of rutile, oxides and orthopyroxene within a glassy matrix. At higher degrees of melting (the granite block), feldspars display a spongy texture throughout and the contact with the glass becomes highly irregular. Quartz grains become increasingly fractured and embayed, although remaining inclusion-free and displaying sharp contacts with the glass.

The glass, commonly perlitic, consists of light-brown and dark-brown phases, and contains microlites of quartz and feldspar, which probably nucleated during rapid cooling. The light brown glass is prevalent in the granite with low degrees of melting (contact zone), whereas the dark brown glass is prevalent in the granite with high degrees of melting (granite block). In thin section, the two glass phases have gradational contacts and hence are not a result

of liquid immiscibility. Rather, they are probably indicative of incomplete liquid-state homogenisation due to both volume diffusion and convection (e.g., [10]).

3. Sampling and analytical methods

Analyses were performed on fresh samples representative of both the melted granite and trachyandesite, along with an unmelted granite sample (6708) of similar lithology to that of the melting region, collected 1 km south of the plug. Crushed rock samples were divided for whole-rock analyses and mineral and glass separations, carried out by conventional magnetic and specific gravity techniques. The final separated mineral and glass fractions were checked for purity and freshness by hand picking under a binocular microscope. Microdrilling was performed using a diamond tipped drill on polished rock chips.

Major element glass analyses were carried out on a polished thin section from samples 6707 and 6700 (Table 1), representing low (10–20%) and high (50–70%) degrees of melting, respectively. Henceforth, for the sake of clarity, we will refer to these samples as LOW and HIGH. The LOW sample is from the contact between the trachyandesite plug and the country granite, whilst the HIGH sample is from the granite block within the plug. To assess the extent of isotopic homogeneity within the glass phase, subsamples (A and B) of each hand specimen (LOW and HIGH) were prepared. The analyses of HIGH subsamples were determined on a 1–0.5 mm glass fraction directly hand picked after sieving (HIGH-A1 and HIGH-B1), and a 100–250 μm glass fraction < 2.4 g/cm^3 (HIGH-A2 and HIGH-B2). The analyses of LOW subsamples were determined on a 100–250 μm glass fraction < 2.4 g/cm^3 (LOW-A and LOW-B). For one subsample, the glass fraction was further subdivided into a relatively less magnetic (LOW-B1) and more magnetic fraction (LOW-B2). The heavy-liquid density of 2.4 g/cm^3 was chosen in order to have pure glass fractions devoid of mineral inclusions.

All analyses were performed at the Vrije Universiteit, Amsterdam. Major element whole-rock analysis of the unmelted granite sample was determined by XRF on a fused glass bead following standard procedures. Mineral and glass analyses were determined using a wavelength dispersive electron microprobe. Sr, Nd and Pb isotope analyses were performed from single sample dissolutions. Roughly

Table 1
Major element (wt%) analyses of the granite and partially melted granite from the Rattlesnake Gulch and estimation of the relative proportions (wt%) of minerals and glass on the basis of major element mass balance

	6708 gr source	6700 HIGH glass	6707 LOW glass
n	1	12	13
SiO_2	72.63	73.51 ± 0.34	78.30 ± 0.33
TiO_2	0.25	0.32 ± 0.01	0.25 ± 0.03
Al_2O_3	14.49	14.04 ± 0.11	12.09 ± 0.13
Fe_2O_3	1.89	1.72 ± 0.05	0.80 ± 0.11
MnO	0.05	0.03 ± 0.01	0.00 ± 0.00
MgO	0.52	0.33 ± 0.04	0.08 ± 0.02
CaO	1.85	0.61 ± 0.03	0.27 ± 0.02
Na_2O	3.39	2.88 ± 0.11	2.14 ± 0.18
K_2O	4.79	6.43 ± 0.15	6.06 ± 0.33
P_2O_5	0.07	bdl	bdl
BaO	0.14	0.14 ± 0.01	bdl
F	nd	bdl	bdl
Cl	nd	bdl	bdl
LOI	0.30	nd	nd
Total [a]	100.37	95.27 ± 0.27	95.18 ± 0.45
ASI	1.02	1.08 ± 0.02	1.13 ± 0.02
Melt and mineral proportions (wt%)			
Quartz	30.51	9.03	23.50
Pl core	13.76	20.53 [b]	13.41
Pl rim	22.72		19.94
K-feld [c]	26.71	1.58	23.19
Biotite	5.85	–	2.74
Opx	–	1.73	1.53
Magnetite	0.41	0.05	0.51
Rutile	–	0.02	0.09
Melt	–	67.06	14.95
Total	99.97	99.99	99.85
SSD	0.0046	0.0443	0.0017

n = number of analyses averaged ± 1 standard deviation; nd = not determined; bdl = below detection limit.

[a] Glass analyses are reported normalised to 100% (the totals are before normalisation). ASI = Alumina Saturation Index, mol $[Al_2O_3/(CaO+Na_2O+K_2O)]$. Glass analyses at grain boundaries with quartz (see Fig. 2) have not been included in the averages.

[b] Average between residual plagioclase core and rim composition.

[c] K-feldspar is orthoclase/microcline in the unmelted granite, anorthoclase in the HIGH glass and sanidine in the LOW glass.

SSD = sum of squared of deviates.

20% of each sample solution was spiked using mixed ^{87}Rb–^{84}Sr, ^{148}Sm–^{150}Nd and separate ^{235}U and ^{208}Pb spikes. The total procedural blanks for Pb, Sr and Nd were < 300, < 200 and < 50 pg, respectively, at the time of these analyses. Pb isotope compositions were measured in static mode and are presented normalised to NIST SRM981, using a fractionation correction of 0.137% per a.m.u. Nd and Sr isotope compositions were measured in dynamic mode, and are presented normalised to $^{86}Sr/^{88}Sr = 0.1194$ and $^{146}Nd/^{144}Nd = 0.7219$, respectively. ^{40}Ar–^{39}Ar step-heating analysis was performed on the groundmass of the trachyandesite sample 6706, to determine eruption age. Analytical procedure is reported elsewhere [24]. Uncertainty, including J factor, in the calculated plateau age is at the 2σ confidence level.

4. Results

The average major element compositions of glasses formed by partial melting of the Rattlesnake Gulch granite are reported in Table 1, along with that of the granite source. The LOW glass has higher contents of K_2O and SiO_2 than the granite source,

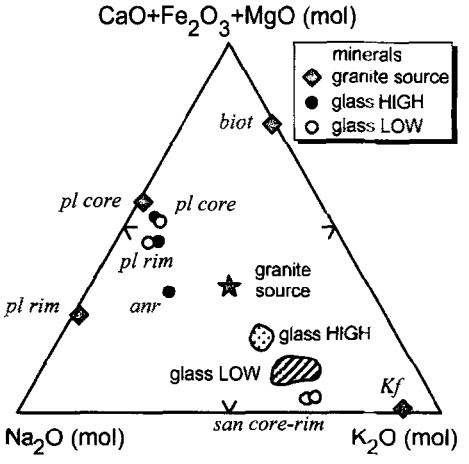

Fig. 1. Na_2O–K_2O–($CaO + Fe_2O_3 + MgO$) triangular diagram (mol%) for the granite, glasses and minerals. Glass analyses at grain boundaries with quartz (see Fig. 2) have not been plotted. *pl* = plagioclase; *Kf* = orthoclase; *san* = sanidine; *anr* = anorthoclase; *biot* = biotite. Mineral compositions represent average compositions (full individual analyses are available from the authors upon request).

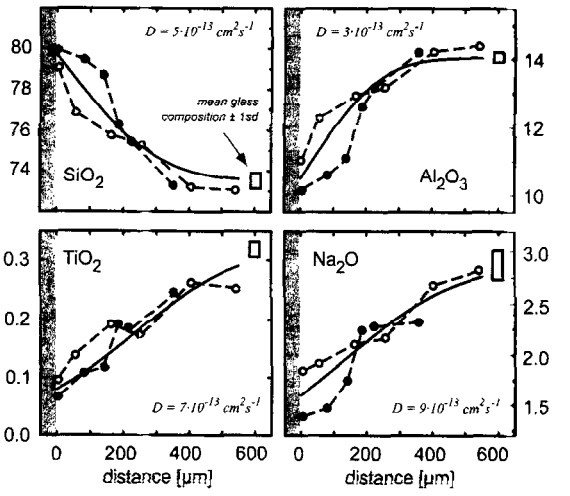

Fig. 2. Glass analyses (dots and circles) at increasing distance from the boundary with two quartz grains in the HIGH glass. The quartz boundary is marked by the grey area. Solid lines represent rough estimates of the effective binary diffusion coefficients [26]. The calculated values ($D \sim 10^{-13}$ cm^2 sec^{-1}) are consistent with results on diffusive quartz dissolution in an andesitic melt [25] extrapolated to 1000–850°C. The time-scale between the onset of melting and the final solidification was set to 14 yr (see thermal model).

because it represents the first melts mainly formed by biotite breakdown (e.g., [23,27]). The HIGH glass has a composition closer to that of the granite source, although it is still enriched in K_2O and SiO_2. The enrichment in the K-feldspar component from biotite breakdown is reflected in both glasses having a higher Alumina Saturation Index than the granite source (ASI, Table 1). Each type of glass has a fairly homogeneous major element composition (Fig. 1) on the sampling scale of the thin section (~ 6 cm^2). Along the contacts with residual minerals, however, even the HIGH glass displays a significant heterogeneity in terms of major elements (Fig. 2), implying diffusion controlled dissolution across a boundary layer at the solid–liquid interface (e.g., [25]).

The extent of melting experienced by the granite has been estimated using major element mass balance calculations based on the compositions of minerals, glasses and granite source, the melting reactions and the observed residual phases. The results, including the relative proportions of minerals in the unmelted granite, are reported in Table 1. The HIGH glass from the granite block inside the plug repre-

Table 2
Sr, Nd and Pb isotope data of the granite and the partially melted granite from the Rattlesnake Gulch

Sample		[Rb] (ppm)	[Sr] (ppm)	[Sm] (ppm)	[Nd] (ppm)	[U] (ppm)	[Pb] (ppm)	$^{87}Sr/^{86}Sr_m$	$^{87}Sr/^{86}Sr_i$	$^{143}Nd/^{144}Nd_m$	ϵNd_i	$^{208}Pb/^{204}Pb_m$	$^{207}Pb/^{204}Pb_m$	$^{206}Pb/^{204}Pb_m$	$^{206}Pb/^{204}Pb_i$
Granite source															
6708	w.r.	230	293	2.953	19.04	9.29	23.2	0.708650 ± 13	0.708266 ± 14	0.512508 ± 5	−2.4	39.098	15.687	19.520	19.471
	duplicate			2.835	18.16			0.708639 ± 11	0.708253 ± 12	0.512497 ± 7	−2.6				
	bomb	235	296	2.935	18.94	9.11	23.1	0.708647 ± 14	0.708259 ± 15	0.512496 ± 9	−2.6	39.086	15.682	19.512	19.465
Glass 6700															
HIGH-A1	HP	288	86.07	3.903	21.96	8.21	23.1	0.709628 ± 12	0.707993 ± 20	0.512507 ± 15	−2.4	39.102	15.683	19.434	19.392
HIGH-A2	< 2.4	299	66.36	3.597	19.60	8.68	23.0	0.710220 ± 10	0.708019 ± 24	0.512513 ± 9	−2.3	39.173	15.707	19.461	19.416
HIGH-B1	HP	273	98.74	4.202	23.61	6.18	24.2	0.709158 ± 14	0.707806 ± 19	0.512505 ± 8	−2.5	39.076	15.678	19.399	19.368
HIGH-B2	< 2.4	278	77.53	3.904	21.76	6.26	24.1	0.709561 ± 9	0.707805 ± 20	0.512502 ± 8	−2.5	39.147	15.699	19.419	19.388
Glass 6707															
LOW-A	< 2.4	427	30.01	2.016	9.964	4.34	19.4	0.715706 ± 11	0.708753 ± 70	0.512510 ± 10	−2.4	38.999	15.708	19.573	19.546
LOW-B1	< 2.4 < magn	352	27.11			3.83	17.5	0.714599 ± 9	0.708244 ± 64			39.058	15.699	19.373	19.347
LOW-B2	< 2.4 > magn	325	29.16			3.77	18.0	0.714326 ± 7	0.708868 ± 55			39.054	15.702	19.351	19.326
Trachyandesite															
6705	w.r.	39.0	1045	6.609	39.19	3.16	13.9	0.705571 ± 9	0.705553 ± 9	0.512550 ± 9	−1.6	38.873	15.664	19.060	19.033
6706	w.r.	53.9	911.4	4.682	26.00	1.83	15.0	0.705700 ± 10	0.705671 ± 10	0.512473 ± 8	−3.1	38.866	15.664	19.056	19.041

Uncertainties in measured (m) and initial (i = 11.9 Ma) isotopic ratios refer to the least significant digits and represent $\pm 2\sigma$ run precision and $\pm 2\sigma$ propagated error, respectively. Uncertainties (2sd) in U/Pb, Rb/Sr and Sm/Nd are ≤ 2%, ≤ 1% and ≤ 0.5%, respectively. The external precision of NIST SRM981 was $^{208}Pb/^{204}Pb = 36.512 \pm 13$, $^{207}Pb/^{204}Pb = 15.431 \pm 4$, $^{206}Pb/^{204}Pb = 16.894 \pm 3$ (2sd, n = 10), that of NIST SRM987 was $^{87}Sr/^{86}Sr = 0.710278 \pm 18$ (2sd, n = 26) and that of the La Jolla standard was $^{143}Nd/^{144}Nd = 0.511852 \pm 10$ (2sd, n = 25). Duplicate analysis of the unmelted granite sample was also performed using a *teflon digestion bomb to check for complete zircon dissolution* and resulted in no significant difference in Nd and Pb isotope ratios. wr = whole rock; HP = hand picked glass fraction directly after sieving; < 2.4 = glass fraction < 2.4 g/cm^3. The glass fraction < 2.4 g/cm^3 of LOW-B has been further subdivided into a relatively less (< magn) and more magnetic (> magn) fraction.

sents ~ 67% melting of the granite with a residue composed of quartz, plagioclase, anorthoclase, orthopyroxene and oxides. The LOW glass from the contact zone of the country granite represents ~ 15% melting of the granite with a residue composed of quartz, plagioclase, sanidine, biotite, orthopyroxene and oxides.

Given the rapid cooling of the shallow-level trachyandesite intrusion (see Section 5.1), the age of granite melting can be reliably dated by the $^{40}Ar-^{39}Ar$ step-heating release spectrum determined on the trachyandesite sample. The $^{40}Ar-^{39}Ar$ plateau (> 90% ^{39}Ar) yields an age of 11.93 ± 0.26 Ma, which is within error of the whole-rock K–Ar age of 11.7 ± 0.7 Ma obtained by Kaczor et al. [22] on the same trachyandesite plug.

Sr, Nd and Pb isotope data for granite, glasses, minerals and trachyandesite are reported in Tables 2 and 3. Significant Sr isotope heterogeneity is observed both within glasses from subsamples of the same hand specimen (dm^3 scale), and between the

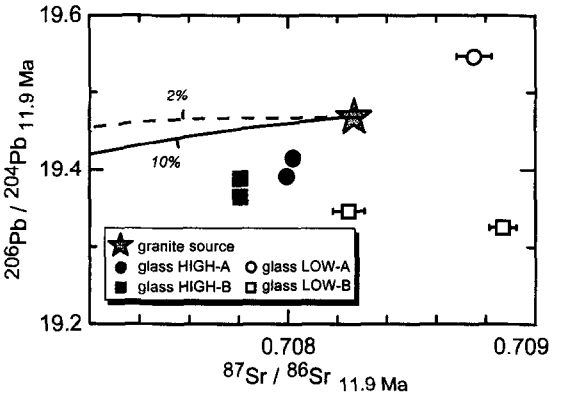

Fig. 3. $^{206}Pb/^{204}Pb$ vs. $^{87}Sr/^{86}Sr$ at 11.9 Ma for the granite and glasses from the Rattlesnake Gulch. 2σ errors are within the symbol size when not plotted. Two limiting case mixing lines between granite melts in isotope equilibrium with their source, and average trachyandesite composition are reported. Sr and Pb concentrations used in the calculation are those of the granite source (solid line) and the average of LOW glasses (dashed line). Figures refer to the mass fraction (wt%) of trachyandesite in the mixture. Clearly the mixing process cannot explain the observed Sr–Pb isotope variations in the glasses.

Table 3
Sr isotope data of minerals from the granite and partially melted granite

Mineral	[Rb] (ppm)	[Sr]	$^{87}Rb/^{86}SR$	$^{87}Sr/^{86}Sr_m$	$^{87}Sr/86Sr_{11.9Ma}$
6708 granite source					
Kf rim	411	523.2	2.270	0.708508 ± 8	0.708124 ± 9
Kf core	305	517.4	1.706	0.707771 ± 14	0.707483 ± 14
pl rim	104	502.1	0.5974	0.706255 ± 10	0.706154 ± 10
pl core	16.7	1112	0.0434	0.705576 ± 9	0.705569 ± 9
Kf	309	481.1	1.856	0.707954 ± 9	0.707640 ± 10
biot	960	31.66	88.78	0.829473 ± 12	0.814470 ± 151
6700 HIGH-A					
pl	69.9	467.0	0.4332	0.707766 ± 14	0.707693 ± 14
anr	106	738.4	0.4152	0.708079 ± 7	0.708009 ± 7
6700 HIGH-B					
anr	122	727.2	0.4842	0.707882 ± 10	0.707800 ± 10
6707 LOW-A					
san	157	378.8	1.199	0.708408 ± 11	0.708205 ± 11
pl	131	536.1	0.7048	0.707979 ± 11	0.707860 ± 11
biot res	94.0	180.2	1.509	0.708634 ± 11	0.708379 ± 11

Minerals of the granite were microdrilled from polished rock chips, whilst minerals of the melted granite were hand picked using a 100–250 μm fraction. pl = plagioclase; Kf = orthoclase; san = sanidine; anr = anorthoclase; biot res = residue after biotite breakdown. Details on uncertainties as in Table 2.

glasses and the granite source (tens of m^3 scale) (Fig. 3). Glasses LOW-A and LOW-B2 have a more radiogenic Sr isotope composition than the granite source at 11.9 Ma, whilst the opposite holds true for samples HIGH-A1, HIGH-A2 and HIGH-B1, HIGH-B2. The absolute $\Delta^{87}Sr/^{86}Sr_{11.9Ma}$ between HIGH and LOW glasses is up to 0.00106 ± 6 (LOW-B2 and HIGH-B2, Table 2). The Sr isotope heterogeneity is coupled, although to a lesser extent, with differences in $^{206}Pb/^{204}Pb_{11.9Ma}$ (Fig. 3), with glass LOW-A having the most radiogenic composition. In contrast, $\epsilon Nd_{11.9Ma}$ of glasses and granite source are within error (Table 2).

5. Discussion

The isotopic heterogeneity on hand specimen scale suggests negligible homogenisation of melts via volume diffusion and convection and hence offers the opportunity to characterise the successive liquid compositions produced during granite melting. Mixing between putative high-silica melts, in isotope equilibrium with the granite source, and the trachyandesite magma could potentially account for some of the observed isotopic variations. Calculations using Pb and Sr isotopes demonstrate, however, that a mixing process is not able to reproduce the isotopic characteristics of the glasses (Fig. 3), in keeping with field observations indicating negligible interaction between the trachyandesite and the granite melts. Our preferred explanation, which we explore in detail below, is that minerals of the granite did not attain Sr and Pb isotope equilibrium during the thermal event and consequently the glasses reflect isotope disequilibrium melting.

5.1. Thermal modelling

An estimate of the time-scale of the melting process is critical in assessing the significance of any isotope (dis)equilibrium. The rate of melt extraction is also crucial, but does not apply to this particular case since melts remained in situ. To estimate the order of magnitude of the time-scale of melting we used a simple one-dimensional explicit finite difference method (e.g., [28]). A granite block, 4 m wide, was placed within the plug according to field relations. Time-dependent temperature profiles are reported in Fig. 4, whilst thermal parameters and boundary conditions are given in the caption. The most pertinent conclusions from the thermal modelling are:

1. the granite block inside the plug reaches the solidus *almost instantaneously* (ca. 3 months);
2. the maximum temperature reached by the granite block is ~ 1000°C after ca. 1.5 yr;
3. the country granite at the contact of the plug does not reach the solidus, although the temperature at 1 m from the contact rises to > 700°C within a few months;

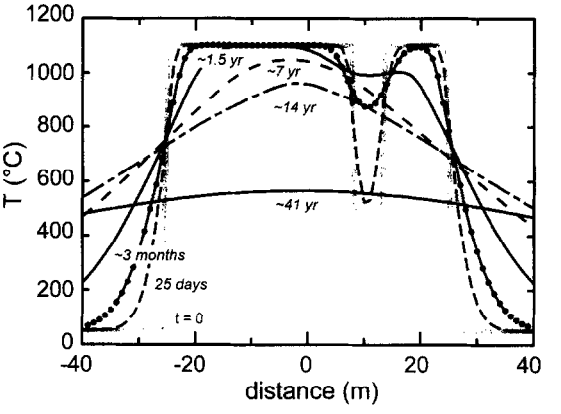

Fig. 4. Temperature–space–time profiles of the cooling trachyandesite plug. Based upon field observations, the plug was assumed to be emplaced instantaneously. The diameter of the plug was set to 50 m, and a block of granite, 4 m wide, was allowed within the plug. The finite difference array was oriented radially from the centre of the plug to the far field boundary (500 m) in the country rock at steps of 1 m. In order for the calculation to be mathematically stable [28], time steps were set to 5 days. Thermal parameters are from Peacock [28] and Huppert and Sparks [29]. The heat of crystallisation of the plug (400 kJ/kg) and the heat of fusion of the granite (300 kJ/kg) were incorporated into the model, allowing for variation in the effective thermal diffusivity, κ (trachyandesite from $9 \cdot 10^{-7}$ to $2.6 \cdot 10^{-7}$ m^2s^{-1}, granite from $1 \cdot 10^{-6}$ to $4.4 \cdot 10^{-7}$ m^2s^{-1}, below and above the solidus, respectively). The onset of melting in the granite was set at 850°C on the basis of a pressure estimate < 0.5 kbar (e.g., [30,31]). This estimate is based on field observations indicating that the plug represents a near surface conduit and the granite was already exposed on the surface prior to the Cenozoic basaltic magmatism [21]. The temperature profile for t = 0 was initialised to the temperatures of the trachyandesite magma and the country granite as a function of the space steps. Magma intrusion temperature was set to 1100°C on the basis of estimates by Kaczor et al. [22] on the eastern trachyandesite plug intruding the Rattlesnake Gulch granite. The country granite temperature was set to a maximum value of 50°C on the basis of the assumed pressure of melting.

4. the temperature of the plug and at the contact with the country granite remains above 500°C for ca. 40 yr.

From experimental petrology data on granites (e.g., [32]), the calculated maximum temperature of ~ 1000°C implies that the granite block should have experienced high degrees of melting (but not total fusion). This is consistent with the geochemical and petrographic characteristics of the HIGH glass and residual minerals.

The estimated temperature at the granite–plug contact, however, does not reach the granite solidus. This contrasts with field observations, indicating significant degrees of melting (LOW glass, Table 1). The reason for the discrepancy is probably due to the assumed boundary conditions: (1) the chosen space step of 1 m does not permit the determination of the temperature within 1 m of the contact; (2) no account is taken of more complex geometries, such as irregular and interfingering contacts, that could have enhanced local melting; (3) the instantaneous injection model does not take into account magma flow through the conduit. This third possibility would maintain the contact temperature at the initial magma temperature (1100°C) and consequently enhance melting within the host granite. In addition, the release of volatiles from both the trachyandesite magma and biotite breakdown in the granite, could have increased the confined volatile pressure along the contact, thus decreasing the solidus of the granite (e.g., [33]).

We can estimate the time-scale necessary to reach the solidus within 0.5 m of the contact for a constant flow of magma (i.e., maintaining the contact temperature at the initial magma temperature) and solving the relative analytical solution [34]:

$$T_i = T_{\text{magma}} \cdot \left[1 - erf\left(\frac{x_i}{\sqrt{i4\kappa t}}\right)\right] \qquad (1)$$

(1)where T_{magma} is the initial magma temperature remaining constant at the contact ($x_i = 0$ m); T_i is the temperature in the country granite at distance x_i from the contact; erf is the error function; κ is the thermal diffusivity of the granite; t is the time elapsed from the intrusion. Eq. (1) indicates that, after approximately 20 days of continuous flow, the temperature at 0.5 m of the contact is > 850°C, the solidus of the granite. In summary, the above explanations, although not included quantitatively in the thermal model, allow for some melting to occur within a few metres of the plug–granite contact, in keeping with field observations.

5.2. Isotope disequilibrium during anatexis

The *essential* requisite to assess the extent of isotope (dis)equilibrium during anatexis is that the relationship between the source rock and the melt can be unequivocally identified. In addition to this, the analytical problem of resolving isotope disequilibrium is made easier in the case of ancient protoliths (Archean or Proterozoic), consisting of minerals with a wide range of parent–daughter isotope ratios (e.g., $^{87}Rb/^{86}Sr$ in feldspar and micas), which have experienced a melting event in the recent past (the last few million years). These conditions ensure the attainment of large isotopic differences, coupled with negligible isotopic age correction to the samples. It is also useful for the crustal sources to have modal proportions of minerals, resulting in a balanced distribution of the element to be studied isotopically (e.g., Sr).

In the case studied, the essential requisite is fulfilled, although the other desirable conditions are only partly met. For example, the time-scale between the formation of the granite protolith and the melting event is relatively short ($\Delta t \sim 80$ Ma). The modal proportion of biotite in the granite source is < 6 wt% (Table 1), and hence < 0.7% of the bulk Sr content has a highly radiogenic signature ($^{87}Sr/^{86}Sr_{11.9Ma} = 0.8145$, Table 3). Given these less than ideal conditions, the Sr isotope heterogeneity among the glasses (Fig. 3) is quite striking. $^{206}Pb/^{204}Pb_{11.9Ma}$ heterogeneity among glasses is also significant (Fig. 3), although not as extreme as Sr isotopes. In contrast, the identical $\epsilon Nd_{11.9Ma}$ of glasses and granite source is an expected result, given the long half-life of ^{147}Sm (106 Ga) and the similar Sm–Nd ratios of major rock-forming minerals in the granite protolith.

The importance of accessory phases preserving Pb isotope heterogeneities during anatexis was discussed by Hogan and Krishna [35]. Here, although not neglecting the observed Pb isotope differences

both within the glasses and between the glasses and the granite source (Fig. 3), we shall focus on the importance of major rock-forming minerals not attaining Sr isotope equilibrium during high-grade thermal events as this isotope disequilibrium is the most marked.

Rb–Sr isotope data on the glasses do not yield an isochron (MSWD = 74, Table 4). Moreover, the errorchron of 3.6 ± 0.5 Ma yielded by the two glasses from subsample LOW-B (~ 70% younger than the actual age), implies that, at the time of melting, the glass fraction with lower Rb/Sr (LOW-B2) had higher $^{87}Sr/^{86}Sr$. This is the opposite to that expected if mixing with the trachyandesite magma were the process responsible for the observed isotopic variations.

Table 4
Isochron regression calculations on glasses and minerals from the partially melted granite

	Age ± 2σ	MSWD
Mineral–Glass HIGH-A		
anr, HIGH-A1, HIGH-A2	11.9 ± 0.2	2.1
anr, pl, HIGH-A1, HIGH-A2	13 ± 6	309
pl, HIGH-A1, HIGH-A2	14 ± 4	11.9
pl, HIGH-A2	13.7 ± 0.2	–
pl, HIGH-A1	14.2 ± 0.2	–
Mineral–Glass HIGH-B		
anr, HIGH-B1, HIGH-B2	11.9 ± 0.2	0.02
Mineral-Glass LOW-A		
biot res, LOW-A	12.6 ± 0.1	–
san, LOW-A	13.5 ± 0.1	–
pl, LOW-A	12.9 ± 0.1	–
san, pl	61 ± 4	–
san, pl, biot res	58 ± 33	4.3
san, pl, biot res, LOW-A	13 ± 9	810
san, biot res	57 ± 3	–
pl, biot res	51 ± 7	–
Glasses		
HIGH-A1, HIGH-A2, HIGH-B1, HIGH-B2 LOW-A, LOW-B1, LOW-B2	14 ± 1	74
LOW-B1, LOW-B2	3.6 ± 0.5	–
LOW-A, LOW-B1, LOW-B2	12 ± 67	216
HIGH-A1, HIGH-A2	12.4 ± 0.8	–
HIGH-B1, HIGH-B2	12 ± 1	–

A minimum uncertainty of ±0.00254% was assumed for the measured $^{87}Sr/^{86}Sr$, based on the external precision of the standard (see Table 2). If the standard error (2σ run precision) of an analysis was > 0.00254%, then the higher value was used. Isochron regressions were calculated with the software ISOPLOT [36] and age estimates are at the 2σ confidence level. pl = plagioclase; Kf = orthoclase; san = sanidine; anr = anorthoclase; biot res = residue after biotite breakdown.

Glass–anorthoclase isochrons of subsamples HIGH-A and HIGH-B are, however, within error of the $^{40}Ar–^{39}Ar$ age (11.9 ± 0.2 Ma for both HIGH-A and HIGH-B, Table 4). This demonstrates that Sr isotope equilibrium was attained on a very local scale (a few centimetres). Subsamples HIGH-A1 and HIGH-B1 have lower Rb/Sr than the density-separated glass fractions HIGH-A2 and HIGH-B2. This suggests that the former (hand picked directly after sieving) could contain feldspar microlites nucleated in isotope equilibrium with the host melt during rapid cooling. The attainment of isotope equilibrium in the residual anorthoclase grains is probably due to their spongy texture, which resulted in a large surface area between mineral and melt and an effective diffusional radius < 50 μm (based on SEM analysis). Average chemical diffusion coefficient of Sr in anorthoclase at 900–1000°C is $\sim 5 \cdot 10^{-14}$ cm^2 s^{-1} [3]. This implies that isotope equilibrium in these grains has been attained in roughly 5 yr [37], in keeping with the estimate of the time over which the granite block has remained above 900°C (Fig. 4).

Despite anorthoclase having attained isotope equilibrium on a local scale, other residual feldspars of the HIGH glasses did not (Tables 3 and 4), even though temperatures reached ~ 1000°C. In particular, mineral–glass pairs from sample HIGH-A yield geologically meaningless ages up to 20% higher than the actual melting age (e.g., pl, HIGH-A2). Mineral–glass and mineral–mineral isotope disequilibrium within the partially melted granite along the contact (LOW-A glass) is the most pronounced. Calculated ages are as much as > 300% higher than the melting age of 11.9 Ma, and tend towards the Cretaceous emplacement age of the granite.

The Sr isotope compositions of minerals and glasses at the time of melting are shown in Fig. 5. These data clearly demonstrate that the residual feldspars contain a population that did not attain Sr isotope equilibrium during melting. An explanation of Sr isotope disequilibrium is provided by the kinetics of solid-state diffusion. On the basis of published Sr diffusion coefficients [2–6], the *almost instantaneous* melting event experienced by the granite (ca. 3 months, Fig. 4) is liable to have allowed negligible resetting of $^{87}Sr/^{86}Sr$ among the major rock-for-

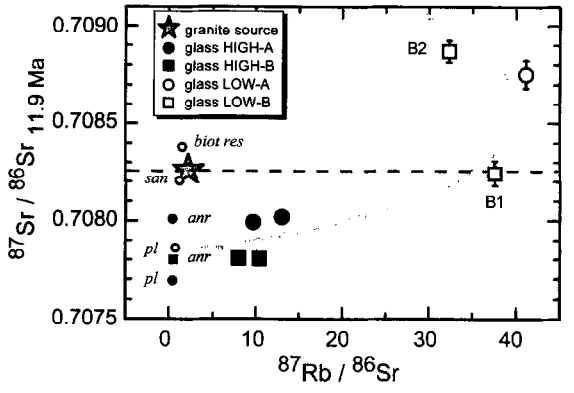

Fig. 5. $^{87}Sr/^{86}Sr$ vs. $^{87}Rb/^{86}Sr$ at 11.9 Ma for the granite, glasses and residual minerals. 2σ errors are within the symbol size when not plotted. Isotope equilibrium conditions during melting would have caused the glasses and residual minerals to have the same $^{87}Sr/^{86}Sr$ of the granite protolith (i.e. to plot along the dashed line). In contrast, the glasses define a trend (grey arrow) consistent with the model proposed in Fig. 6. Smaller symbols refer to residual minerals from the corresponding glass: *san* = sanidine, *anr* = anorthoclase, *pl* = plagioclase, *biot res* = residue after biotite breakdown.

ming minerals. Consequently, the onset of melting in the granite resulted in a liquid phase whose Sr isotope composition depended on the relative proportion of minerals contributing to the melt, along with the solid–liquid distribution coefficient (K_d) of Sr for each mineral (i.e., the Sr budget provided to the melt by each mineral).

As a schematic example, we show the composition of successive liquid fractions formed by biotite and plagioclase melting in the case of no isotope equilibration and considering each mineral separately (Fig. 6). Liquid fractions will have $^{87}Sr/^{86}Sr$ corresponding to that of the mineral (biotite or plagioclase) from which they are derived (grey arrows). The Rb/Sr will depend on the relative degree of melting (e.g., F_{biot}) and the K_d^{Sr}/K_d^{Rb}. This means that as $F_{biot} \rightarrow 0$, the Rb/Sr of liquids originating from biotite will be low and will approach that of biotite as $F_{biot} \rightarrow 1$. The opposite sense holds true for plagioclase. The liquid fractions from plagioclase and biotite melting, provided they are homogenised, will exhibit intermediate $^{87}Sr/^{86}Sr$ and Rb/Sr (dashed lines, Fig. 6), according to the relative Rb and Sr budget provided to the melt by each mineral. If incomplete liquid-state homogenisation occurs, or the first melts are rapidly extracted from the source, we would expect to find a succession of distinct liquid fractions, originating from the same source, that have variable Rb/Sr and $^{87}Sr/^{86}Sr$ (thick curved arrow). Only by chance, therefore, will the Sr isotope composition of a given liquid fraction be identical to that of the source rock. The presence of other major rock-forming minerals (e.g., K-feldspar) and isotopic zonation (e.g., plagioclase core and rim, Table 3) will complicate the diagram but not modify the conclusion.

In the case studied, the presence of isotopically distinct glass fractions is indicative of incomplete homogenisation of the melts. The evolution pattern of the glasses observed in Fig. 5, corresponds to that predicted by the model (Fig. 6). The glass with $^{87}Sr/^{86}Sr$ more radiogenic than the granite source and with the highest Rb/Sr (LOW-A) represents a liquid fraction originating at the onset of melting from biotite breakdown. The two glass subsamples with different magnetic susceptibility (LOW-B1 and LOW-B2) represent different liquid fractions at the onset of melting: the more magnetic fraction (LOW-B2) has the most radiogenic $^{87}Sr/^{86}Sr$ and a lower Rb/Sr than the less magnetic fraction (LOW-B1).

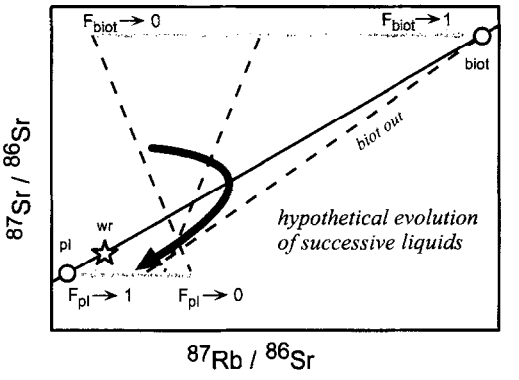

Fig. 6. Schematic diagram illustrating the effects of Sr isotope disequilibrium during anatexis. This model considers melting of biotite and plagioclase without any isotopic resetting (see text). Solid line = pre-melting isotopic relationship between plagioclase and biotite (also reported is the composition of the hypothetical whole rock). Grey arrows = compositions of liquids from biotite and plagioclase considering a degree of melting of the relative mineral ($F_{biot,\ pl}$) from 0 to 1. Dashed lines = possible compositions of mixtures of liquid fractions originating from biotite and plagioclase melting. Thick curved arrow = hypothetical evolution of successive liquid fractions if melts are rapidly extracted from the source or are chemically isolated.

This is consistent with LOW-B2 representing a liquid phase produced from a greater proportion of biotite (thus relatively more magnetic) contributing to the Rb–Sr budget of the melt than LOW-B1 (Fig. 6). At higher degrees of melting the glass subsamples HIGH-A and HIGH-B have less radiogenic $^{87}Sr/^{86}Sr$, although still higher Rb/Sr, than the granite source. This implies that feldspars were the dominant minerals contributing to the Rb–Sr budget of these melt fractions.

6. Implications

The most significant result of this study is the marked Sr isotope disequilibrium both within the different glass fractions and between the glasses and the granite source (Fig. 5). Undoubtedly, this geological setting is *atypical* of granitoid petrogenesis, in that melts were frozen in the site of formation and did not rise through the crust and form pluton-size igneous bodies. However, this has enabled us to study crustal melting in a geologic setting with an unambiguous source–melt relationship, and to identify isotopically different liquids reflecting a disequilibrium melting process. The important question raised by these data is: to what extent is it possible to extrapolate the results to the genesis of crustal melts and, more generally, to studies of regional metamorphic terranes?

In general, the extent of isotope equilibration between rock-forming minerals *before* the onset of melting is mainly controlled by: (1) the time-scale between the closure temperatures of minerals and the onset of melting and (2) the rate of elemental diffusion between adjacent mineral phases. *After* melting is initiated, the main parameters controlling the extent of isotope equilibration are: (1) the duration of high-temperature regimes above closure temperatures; (2) the rate of melting; (3) the rate of melt extraction; and (4) the rate of elemental diffusion between mineral and melt phases.

The Sr isotope data on the glasses and granite source demonstrate disequilibrium on both the outcrop (a few tens of m^3) and hand specimen (a few dm^3) scales. Recent studies on melt segregation in the continental crust [38,39] provided evidence for rapid extraction (10^2–10^4 yr) of small melt fractions once the permeability threshold has been reached (e.g., [40]) and well below the rheologically critical melt percentage (e.g., [41]). Consequently, incomplete isotopic resetting between adjacent mineral phases *before* the onset of melting (as in our study), coupled with rapid rates of melt extraction, will prevent isotope equilibration *after* melting is initiated. The net result is the production of isotopically distinct batches of melts that do not mirror the isotopic composition of the source region.

The generation of crustal melts by basalt underplating, a process akin to the case studied, occurs in time-scales of 10^2–10^3 yr [29]. This is a rapid process, significantly shorter than the time-scales of 10^6–10^7 yr implied for the production of crustal melts due to crustal thickening alone [42], and will generally limit the possibility for isotope equilibration. Thus, anatexis by basalt underplating can potentially produce melts in isotope disequilibrium with their sources.

The temperature reached during melting of the Rattlesnake granite, although for only 5 yr, was extremely high ($\sim$ 1000°C), and uncommon during anatexis caused by collisional tectonics [27,42]. Consequently, the diffusion coefficient of Sr in feldspar should have been increased by approximately 3–4 orders of magnitude [2–6], relative to more *typical* crustal melting temperatures (700–800°C). Despite this fact, residual feldspars maintained Sr isotope heterogeneities and melts are in strong isotope disequilibrium with their source (Fig. 5). At temperatures typical of anatexis in orogenic belts, diffusion calculations [37] establish that the time required to achieve Sr isotope equilibrium in feldspar grains of medium and coarse grained (0.1–1 cm) rocks is between a few million and several tens of millions of years. In feldspar porphyroblasts ($>$ 1 cm) a time in excess of 100 Ma may be required. This suggests that isotope disequilibrium during high-grade metamorphism and anatexis may be important even in long lived (10^6–10^7 yr) regional metamorphic settings.

These observations have important implications for the petrogenesis of granitoids. Closure temperature, and by inference diffusion coefficient, of Nd in garnet [12–17] is comparable to or even higher than that of Sr in feldspar (depending on the composition of the latter), making this mineral liable to retain its isotopic signature during thermal events even for

tens of millions of years. This implies that old garnet-bearing crustal sources can potentially produce melts with significant heterogeneities in terms of Nd isotopes. As such, we cannot rule out a priori that Nd isotopes, on which models to infer the ratio of mantle vs. crustal components in granitoids rely (e.g., [43]), are not susceptible to isotope disequilibrium during anatexis. Equally, current models for the assimilation of crustal material by basalts [44] may need to be re-considered, as also suggested by Knesel and Davidson [10] and Tommasini and Davies [11]. Furthermore, the preservation of isotopic heterogeneities between mineral phases during high-grade thermal events prevents reliable radiometric dating, because the fundamental assumption of isotope equilibrium does not apply. Mineral–whole rock or mineral–mineral pairs will yield erroneous ages (Table 4), as observed in other geological settings of high-grade terranes (e.g., [45]). Clearly, a better assessment of the extent of isotope (dis)equilibrium in crustal rocks during high-grade thermal events is critical to our understanding of igneous and metamorphic processes.

Acknowledgements

We would like to thank R. Carlson, D. Cherniak and J. Davidson for their constructive reviews. This paper has greatly benefited from discussion with A. Heumann and T. Elliott. We are particularly grateful to I.S.E. Charmichael and R.A. Lange for assistance during field work. This research was supported by EU grant ERBCHBICT941222 to S.T. We wish to thank W.J. Lustenhouwer and J.R. Wijbrans for help during microprobe and Ar–Ar analyses. Facilities for isotopic and microprobe analyses were provided by the Vrije Universiteit Amsterdam and by the Netherlands Organisation for Scientific Research (NWO). This is NSG publication # 970111. *[UC]*

References

[1] J.B. Brady, Diffusion data for silicate minerals, glasses, and liquids, in: T.J. Ahrens (Ed.), Mineral Physics and Crystallography. A handbook of physical constants, AGU, Washington DC, 1995, pp. 269–290.

[2] B.J. Giletti, Rb and Sr diffusion in alkali feldspars, with implications for cooling histories of rocks, Geochim. Cosmochim. Acta 55 (1991) 1331–1343.

[3] D.J. Cherniak, E.B. Watson, A study of strontium diffusion in K-feldspar, Na–K feldspar and anorthite using Rutherford backscattering spectroscopy, Earth Planet. Sci. Lett. 113 (1992) 411–425.

[4] D.J. Cherniak, F.J. Ryerson, A study of strontium diffusion in apatite using Rutherford Backscattering spectroscopy and ion implantation, Geochim. Cosmochim. Acta 57 (1993) 4653–4662.

[5] D.J. Cherniack, E.B. Watson, A study of strontium diffusion in plagioclase using Rutherford backscattering spectroscopy, Geochim. Cosmochim. Acta 58 (1994) 5179–5190.

[6] B.J. Giletti, J.E.D. Casserly, Strontium diffusion kinetics in plagioclase feldspars, Geochim. Cosmochim. Acta 58 (1994) 3785–3793.

[7] G.R. Davies, A.N. Halliday, G.A. Mahood, C.M. Hall, Isotopic constraints on the production rates, crystallisation histories and residence times of pre-caldera silicic magmas, Long Valley, California, Earth Planet. Sci. Lett. 125 (1994) 17–37.

[8] S.N. Feldstein, A.N. Halliday, G.R. Davies, C.M. Hall, Isotope and chemical microsampling: Constraints on the history of an S-type rhyolite, San Vincenzo, Tuscany, Italy, Geochim. Cosmochim. Acta 58 (1994) 943–958.

[9] T. Hammouda, M. Pichavant, M. Chaussidon, Isotopic equilibration during partial melting: an experimental test of the behaviour of Sr, Earth Planet. Sci. Lett. 144 (1996) 109–122.

[10] K.M. Knesel, J.P. Davidson, Isotopic disequilibrium during melting of granite and implications for crustal contamination of magmas, Geology 24 (1996) 243–246.

[11] S. Tommasini, G.R. Davies, Isotopic disequilibrium during anatexis: consequences for radiogenic isotope systematics, Terra 7 (1995) 299.

[12] K. Mezger, G.N. Hanson, S.R. Bohlen, U–Pb systematics of garnet: Dating the growth of garnet in the late Archean Pikwitonei granulite domain at Cauchon and Natawahunan Lakes, Manitoba, Canada, Contrib. Mineral. Petrol. 101 (1989) 136–148.

[13] K.W. Burton, R.K. O'Nions, High-resolution garnet chronometry and the rates of metamorphic processes, Earth Planet. Sci. Lett. 107 (1991) 649–671.

[14] K. Mezger, C.M. Rawnsley, S.R. Bohlen, G.N. Hanson, U–Pb garnet, sphene, monazite and rutile ages: Implications for the duration of high-grade metamorphism and cooling histories, Adirondack Mts., New York, J. Geol. 99 (1991) 415–428.

[15] K. Mezger, E.J. Essene, A.N. Halliday, Closure temperature of the Sm–Nd system in metamorphic garnets, Earth Planet. Sci. Lett. 113 (1992) 397–409.

[16] D. Vance, R.K. O'Nions, Prograde and retrograde thermal histories from the central Swiss Alps, Earth Planet. Sci. Lett. 114 (1992) 113–129.

[17] K.W. Burton, M.J. Kohn, A.S. Cohen, R.K. O'Nions, The relative diffusion of Pb, Nd, Sr and O in garnet, Earth Planet. Sci. Lett. 133 (1995) 199–211.

[18] T.E. Krogh, Improved accuracy of U–Pb zircon ages by the creation of more concordant systems using an air abrasion technique, Geochim. Cosmochim. Acta 46 (1982) 637–649.
[19] P. Copeland, T.M. Harrison, R.R. Parrish, B.C. Burchfiel, K.V. Hodges, Identification of inherited-radiogenic Pb in monazite and its implications for U–Pb systematics, Nature 333 (1988) 760–763.
[20] L.S. Zhang, U. Schärer, Inherited Pb components in magmatic titanite and their consequences for the interpretation of U–Pb ages, Earth Planet. Sci. Lett. 138 (1996) 57–65.
[21] C.W. Chesterman, Volcanic geology of the Bodie Hills, Mono County, California, GSA Mem. 116 (1968) .
[22] S.M. Kaczor, G.N. Hanson, Z.E. Eterman, Disequilibrium melting of granite at the contact with a basic plug: a geochemical and petrographic study, J. Geol. 96 (1988) 61–78.
[23] Y. Al-Rawi, I.S.E. Carmichael, A note on the natural fusion of granite, Am. Mineral. 52 (1967) 1806–1814.
[24] J.R. Wijbrans, M.S. Pringle, A.A.P. Koppers, R. Scheveers, Argon geochronology of small samples using the Vulkaan argon laserprobe, Proc. Kon. Ned. Akad. Wetensch. 98 (1995) 185–218.
[25] Y. Zhang, D. Walker, C.E. Lesher, Diffusive crystal dissolution, Contrib. Mineral. Petrol. 102 (1989) 492–513.
[26] A.W. Hofmann, Diffusion in natural silicate melts: a critical review, in: R.B. Hargraves (Ed.), Physics of Magmatic Processes, Princeton Univ. Press, Princeton, 1980, pp. 385–417.
[27] J.D. Clemens, V.D. Vielzeuf, Constraints on melting and magma production in the crust, Earth Planet. Sci. Lett. 86 (1987) 287–306.
[28] S.M. Peacock, Thermal modeling of metamorphic pressure–temperature–time paths: A forward approach, in: F.S. Spear, S.M. Peacock (Eds.), Metamorphic Pressure–Temperature–Time Paths. Short Course in Geology, AGU, Washington DC, 1989, pp. 57–102.
[29] H.E. Huppert, R.S.J. Sparks, The generation of granitic magmas by intrusion of basalt into continental crust, J. Petrol. 29 (1988) 599–624.
[30] A. Ebadi, W. Johannes, Beginning of melting and composition of first melts in the system Qz–Ab–Or–H_2O–CO_2, Contrib. Mineral. Petrol. 106 (1991) 286–295.
[31] S.R. Bohlen, J.O. Eckert, W.B. Hankins, Experimentally determined solidi in the Ca-bearing granite system $NaAlSi_3O_8$–$CaAl_2Si_2O_8$–$KAlSi_3O_8$–SiO_2–H_2O–CO_2, Am. Mineral. 80 (1995) 752–756.
[32] D.B. Clarke, Granitoid Rocks, Chapman and Hall, London, 1992.
[33] B.A. Litvinovskiy, Y.Y. Podladchikov, A.N. Zanvilevich, V.M. Dunichev, Melting of acid volcanites in contact with a shallow basic magma, Geokhimiya 6 (1990) 807–814.
[34] H.S. Carslaw and J.C. Jaeger, Conduction of heat in solidus, Clarendon, Oxford, 1959, 510 pp.
[35] J.P. Hogan, A. Krishna Sinha, The effect of accessory minerals on the redistribution of lead isotopes during crustal anatexis: A model, Geochim. Cosmochim. Acta 55 (1991) 335–348.
[36] K.R. Ludwig, Isoplot 2.71: A plotting and regression program for radiogenic isotope data, US Geol. Surv. Open File Rep. 44 (1994) 91–445.
[37] J. Crank, The Mathematics of Diffusion, Oxford Univ. Press, Oxford, 1975, 414 pp.
[38] N. Petford, J.R. Lister, R.C. Kerr, The ascent of felsic magmas in dykes, Lithos 32 (1994) 161–168.
[39] E.W. Sawyer, Melt segregation in the continental crust, Geology 22 (1994) 1019–1022.
[40] S. Maaløe, Principles of Igneous Petrology, Springer, Berlin, 1985, 374 pp.
[41] A.A. Arzi, Critical phenomena in the rheology of partly melted rocks, Tectonophysics 44 (1978) 173–184.
[42] P.C. England, A.B. Thompson, Pressure–temperature–time paths of regional metamorphism I. Heat transfer during evolution of regions of thickened continental crust, J. Petrol. 25 (1984) 894–928.
[43] G.L. Farmer, Magmas as tracers of lower crustal composition: an isotopic approach, in: D.M. Fountain, R. Arculus, R.W. Kay (Eds.), Continental Lower Crust, Elsevier, Amsterdam, 1992, pp. 363–390.
[44] D.J. DePaolo, Trace element and isotopic effects of combined wallrock assimilation and fractional crystallisation, Earth Planet. Sci. Lett. 53 (1981) 189–202.
[45] M. Thöni, E. Jagoutz, Some new aspects of dating eclogites in orogenic belts: Sm–Nd, Rb–Sr, and Pb–Pb isotopic results from the Austroalpine Saualpe and Koralpe type-locality (Carinthia/Styria, southeastern Austria), Geochim. Cosmochim. Acta 56 (1992) 347–368.